

Geophysical Research Letters[®]

RESEARCH LETTER

10.1029/2022GL097900

Key Points:

- Descent rate data used for navigation by one deep float model serendipitously reveal vertical velocity signatures of internal waves
- Deep internal wave vertical velocities average root mean square variances are $\sim 0.0045 \text{ m s}^{-1}$ and dominant vertical wavelengths are $\sim 757 \text{ m}$
- Vertical velocity variances and dominant vertical wavelengths exhibit geographical patterns, varying among and within deep ocean basins

Correspondence to:

G. C. Johnson,
gregory.c.johnson@noaa.gov

Citation:

Johnson, G. C., Whalen, C. B., Purkey, S. G., & Zilberman, N. (2022). Serendipitous internal wave signals in Deep Argo data. *Geophysical Research Letters*, 49, e2022GL097900. <https://doi.org/10.1029/2022GL097900>

Received 14 JAN 2022
Accepted 18 MAR 2022

Author Contributions:

Conceptualization: Gregory C. Johnson
Formal analysis: Gregory C. Johnson
Funding acquisition: Gregory C. Johnson, Sarah G. Purkey, Nathalie Zilberman
Investigation: Gregory C. Johnson
Methodology: Gregory C. Johnson
Project Administration: Gregory C. Johnson, Sarah G. Purkey, Nathalie Zilberman
Resources: Gregory C. Johnson, Sarah G. Purkey, Nathalie Zilberman
Software: Gregory C. Johnson
Supervision: Gregory C. Johnson
Validation: Gregory C. Johnson
Visualization: Gregory C. Johnson
Writing – original draft: Gregory C. Johnson, Caitlin B. Whalen
Writing – review & editing: Gregory C. Johnson, Caitlin B. Whalen, Sarah G. Purkey, Nathalie Zilberman

© 2022. American Geophysical Union.
All Rights Reserved.

Serendipitous Internal Wave Signals in Deep Argo Data

Gregory C. Johnson¹ , Caitlin B. Whalen² , Sarah G. Purkey³ , and Nathalie Zilberman³ 

¹NOAA/Pacific Marine Environmental Laboratory, Seattle, WA, USA, ²Applied Physics Laboratory, University of Washington, Seattle, WA, USA, ³Scripps Institution of Oceanography, University of California San Diego, La Jolla, CA, USA

Abstract Serendipitous measurements of deep internal wave signatures are evident in oscillatory variations around the background descent rates reported by one model of Deep Argo float. For the 10,045 profiles analyzed here, the average root-mean-square of vertical velocity variances, $\sqrt{\langle w'^2 \rangle}$, from 1,000 m to the seafloor, is 0.0045 m s^{-1} , with a 5%–95% range of 0.0028 – 0.0067 m s^{-1} . Dominant vertical wavelengths, λ_z , estimated from the integrals of lagged autocorrelation sequences have an average value of 757 m , with a 5%–95% range of 493 – $1,108 \text{ m}$. Both $\sqrt{\langle w'^2 \rangle}$ and λ_z exhibit regional variations among and within some deep ocean basins, with generally larger $\sqrt{\langle w'^2 \rangle}$ and shorter λ_z in regions of rougher bathymetry or stronger deep currents. These correlations are both expected, since larger $\sqrt{\langle w'^2 \rangle}$ and shorter λ_z should be found near internal wave generation regions.

Plain Language Summary Ocean density increases with increasing depth, supporting internal waves below the ocean surface. These internal waves are generated near the surface by varying wind forcing such as passing storms and near the bottom by interactions of currents (including tidal) with rough bathymetry (such as seamounts and ridges). They can travel for long distances in both the vertical and the horizontal. When they break, they play important roles in mixing temperature, salinity, and other water properties. Deep Argo is an observing system designed to measure temperature and salinity profiles from the surface to the bottom of the ocean. One model of Deep Argo float serendipitously observes internal wave signals as variations in descent rate data, which it collects primarily for navigation purposes, from the surface to the seafloor. These observations reveal patterns in the magnitudes of these internal wave signals, with stronger internal wave activity near continental rises and mid-ocean ridges and lower levels over smoother abyssal plains. Also, regions with strong deep flows, such as the Samoan Passage through which bottom water is funneled into the North Pacific, or the region south of the Campbell Plateau through which the Antarctic Circumpolar Current flows, exhibit stronger deep internal wave signatures.

1. Introduction

Internal waves are nearly ubiquitous in the oceans (e.g., Alford et al., 2016; Garrett & Munk, 1979; Nikurashin & Ferrari, 2013), carrying energy vertically from the surface downward and from the seafloor upward, as well as horizontally, in some instances across ocean basins. Internal wave breaking ultimately dissipates much of the wind and tidal energy in the oceans (Kunze, 2017; Waterhouse et al., 2014), and deep internal wave mixing drives water-mass transformations important to the global deep ocean circulation (de Lavergne et al., 2016; Kunze, 2017; Munk & Wunsch, 1998; Nikurashin & Ferrari, 2013). Internal waves are often measured either from time series of isotherms (analyzing their vertical displacements or vertical strain) or horizontal velocity (analyzing the velocities or vertical shear of those velocities) (e.g., Alford et al., 2016). Here we use descent rate data from Deep Argo floats collected primarily for navigational purposes to assess the amplitude of vertical velocities and vertical wavelengths of internal waves in the water column below the thermocline.

Deep Argo is a relatively new mission for the Argo program, designed to regularly sample the global ocean below the 2,000-dbar pressure limit of core Argo floats, and hence improve monitoring of variations in ocean temperature, salinity, and currents (Johnson et al., 2015). Float models capable of profiling to 4,000 and 6,000 dbar have been designed and successfully deployed in regional pilot arrays (Roemmich, Alford et al., 2019; Roemmich, Sherman et al., 2019), quantifying recent warming of bottom waters of Antarctic origin in the Southwest Pacific (Johnson et al., 2019) and Brazil basins (Johnson et al., 2020), detecting temperature-salinity variability near Antarctic Bottom Water formation regions (Foppert et al., 2021; Thomas et al., 2020), and allowing detailed analyses of deep ocean circulation (Zilberman et al., 2020). A 6,000-dbar profiling capability allows sampling from the ocean surface to the seafloor over 98% of the ocean area and 97% of the ocean volume, with the exceptions

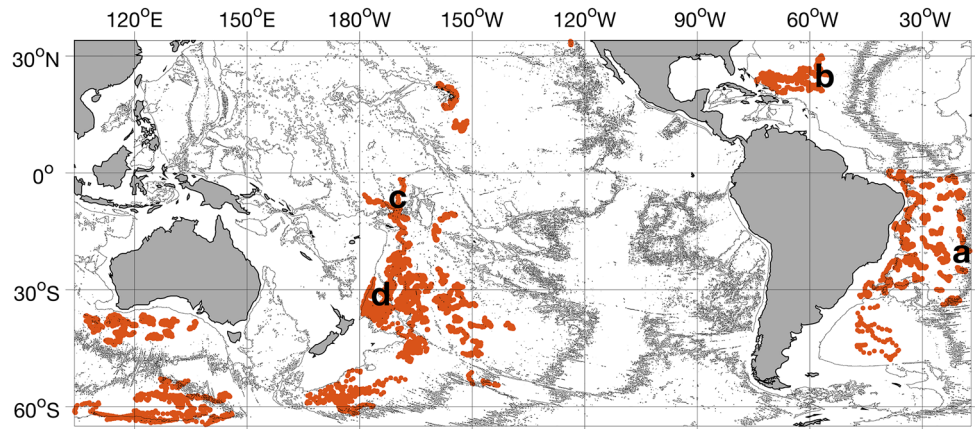


Figure 1. Locations of the 10,045 Deep SOLO profiles (orange dots) analyzed here with the 4,000 m isobath (black contours) from ETOPO2 (Smith & Sandwell, 1997). Locations of example profiles in Figure 2 are indicated by letters a–d.

being a few very deep ocean trenches, and small portions of the ocean immediately above the deepest abyssal plains.

At the start of its descent phase, the Deep Sounding Oceanographic Lagrangian Observer (SOLO) float model (Roemmich, Alford et al., 2019; Roemmich, Sherman et al., 2019) pumps all of the oil from its external bladder to its internal reservoir that is required to target a 0.07 m s^{-1} descent rate when it reaches the bottom. Hence, it sinks most rapidly (order 0.25 m s^{-1}) in the lightest waters near the surface, and steadily slows as it descends into denser waters. The float controller, batteries, and buoyancy engine are inside mated 13" diameter glass hemispheres protected by plastic hard-hat housings, with the CTD (conductivity-temperature-depth) instrument in a smaller externally mounted titanium cylinder. Pressure samples are taken typically at between 5 and 50-dbar pressure intervals, depending on software settings, to monitor the descent rate. A 3-m wire rope dangling from the float brakes its descent as the rope lays down on the bottom, preventing the CTD on the float from contacting the seafloor.

Initial examinations of vertical descent velocities from Deep SOLO float profiles readily revealed signatures of internal waves as oscillations around what would have otherwise been a steady deceleration with increasing pressure. The float-measured oscillations have average root-mean-square (RMS) amplitudes of $\sim 0.0045 \text{ m s}^{-1}$ and average dominant vertical wavelengths of $\sim 757 \text{ m}$ in the water column below 1,000 m. Here we explore regional variations in the amplitudes and wavelengths of these serendipitous observations of internal wave signals among and within the basins sampled by Deep Argo regional pilot arrays using Deep SOLO floats.

2. Data and Methods

Deep SOLO floats measure pressure and time during descent nominally at 5 to 50-dbar pressure intervals, depending on how engineering parameters are set for an individual float. These measurements are telemetered to shore when the float surfaces during each nominally 10-day cycle. We only use data (Argo, 2021) from profiles that sample to at least 2,995 m, and limit our analysis to pressures greater than 800 m, below the main pycnocline in the regions analyzed. We also remove three profiles with vertical gaps in these descent rate data that are too long to interpolate through and 10 more profiles after visual inspection. The screening leaves 10,045 profiles, mostly in the Brazil Basin and the Southwest Pacific Basin, but also in the South Australian Basin, the Australian-Antarctic Basin, the North American Basin, and a few in the Central and Northeast Pacific basins (Figure 1).

For each profile extending to at least 2,995 m we estimate vertical velocities from first differences of depths (derived from pressure measurements) divided by those of times (Figure 2, gray dots). We discard the three deepest estimates to avoid bottom interactions, then apply a LOESS smoother (Cleveland & Devlin, 1988) with a half-power point of $\sim 150 \text{ m}$ to estimate vertical velocities on a regular grid at 10-m intervals from 1,000 m to the deepest pressure (Figure 2, black lines), smoothing over truncation noise in the raw data.

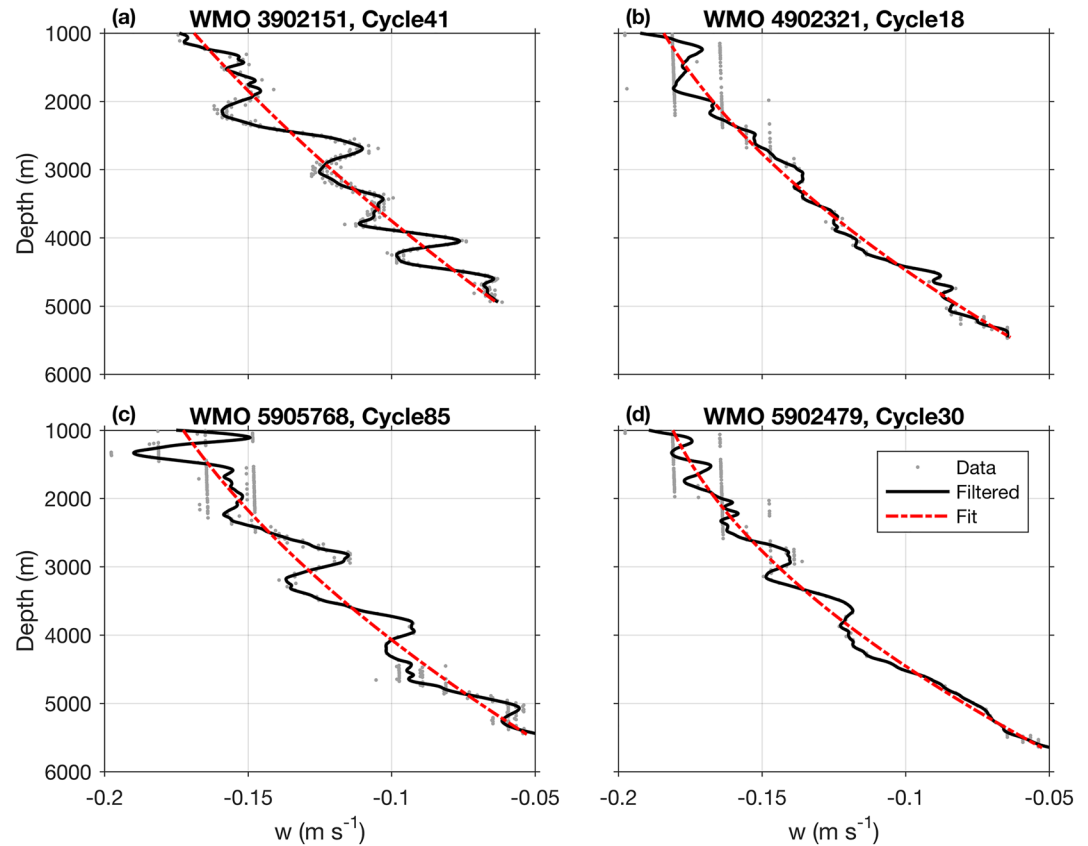


Figure 2. (a) Descent rates of 4 example profiles with raw data from first differences of pressure over time (gray dots), values at 10 m intervals derived by filtering raw data with a 150 m lengthscale LOESS smoother (black curves), and background values (red dashed lines) estimated from a second order polynomial fits to the filtered values versus pressure below 1,000 m. Located (a) on the western flank of the Mid-Atlantic Ridge in the Brazil Basin, (b) on the abyssal plain of the North Atlantic Basin, (c) in the Central Pacific Basin north of the Samoan Passage, and (d) in the interior of the Southwest Pacific Basin (locations at corresponding letters on Figure 1).

We then fit a second-order polynomial to these gridded vertical velocities as an estimate of the background fall rate that steadily decreases with increasing pressure (Figure 2, red dot-dashed lines), and subtract those background fall rates from each profile to yield the residual vertical velocities (hereafter w') relative to the background fall rates. This simple model is suitable because the analysis is started at 1,000 m, well below the permanent pycnocline, where temperature variations are small, and in situ density increases relatively steadily with pressure. Since Deep SOLO floats do not make buoyancy adjustments during descent, unlike some other profiling floats, a flight model (e.g., Cusack et al., 2017) is not needed to interpret variations around the background profiling rate as oceanic vertical velocities. Typical background fall rates are about $0.17 (\pm 0.01) \text{ m s}^{-1}$ at 1,000 m, and decrease nearly linearly to about $0.07 (\pm 0.01) \text{ m s}^{-1}$ at profile maximum depths, where the uncertainties (here and throughout) are one standard deviation.

We calculate the average RMS deep w' variances averaged from 1,000 m to the maximum depth analyzed for each profile, hereafter $\sqrt{\langle w'^2 \rangle}$. We also estimate the dominant vertical wavelength of w' for each profile, hereafter λ_z , as 2π times the maximum of the one-sided integral of the lagged autocorrelation of w' , starting the integral from the maximum correlation (zero lag).

We also examine the correlation of $\sqrt{\langle w'^2 \rangle}$ and λ_z with local bathymetric roughness (e.g., Gille et al., 2000). We estimate it as the square root of the variance of ocean bathymetry (GEBCO Compilation Group, 2021) at 1' resolution within 40 km square bins on a $0.25^\circ \times 0.25^\circ$ grid, and use the resulting map to interpolate it to float profile locations.

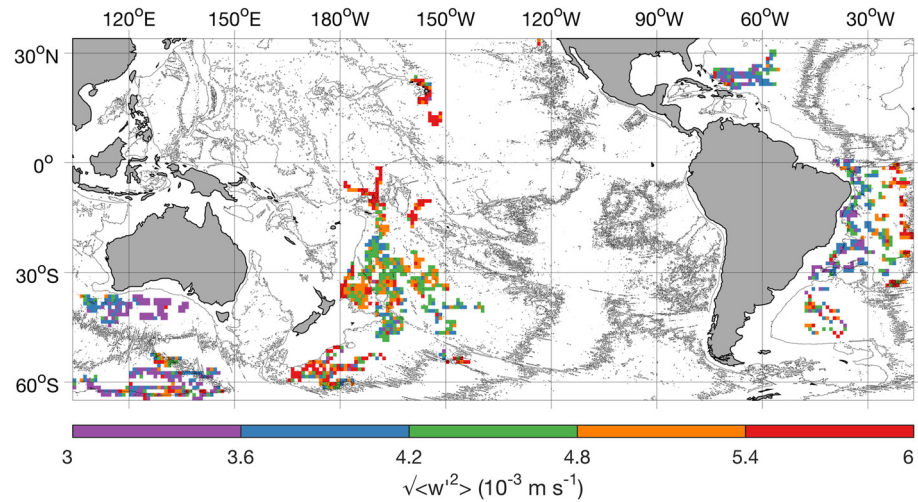


Figure 3. Mean deep RMS w' variances, $\sqrt{\langle w'^2 \rangle}$, from 1,000 m to the bottom pressure of deep SOLO profiles averaged in 1° latitude \times 1° longitude bins.

3. Results

For all 10,045 profiles analyzed $\sqrt{\langle w'^2 \rangle}$ has an average value of $4.5 (\pm 1.2) \times 10^{-3} \text{ m s}^{-1}$. The distribution of $\sqrt{\langle w'^2 \rangle}$ is slightly skewed toward large values, with a median of 4.4×10^{-3} , a fifth percentile of 2.8×10^{-3} , and a 95th percentile of $6.7 \times 10^{-3} \text{ m s}^{-1}$. The λ_z values have an average of $757 (\pm 193) \text{ m}$. Their distribution is slightly skewed toward longer values, with a median of 731, fifth percentile of 493, and 95th percentile of 1,108 m. This distribution should be regarded with some caution because Doppler effect errors result from profiling through propagating waves as explored in Section 4, the energy of lowest vertical modes may be underestimated by removing a background descent rate that is a quadratic function of pressure, and profiles collected in shallower water will not resolve longer vertical wavelengths.

The $\sqrt{\langle w'^2 \rangle}$ values (Figures 2b and 3) are generally lower than average for the profiles in the North American Basin of the western North Atlantic Ocean, with a few higher values adjacent to the Caribbean Islands. The λ_z values there are noticeably longer than average (Figures 2b and 4). These patterns are consistent with little local generation or scattering of internal waves on the abyssal plain, which is very smooth, and propagation of internal waves generated a long distance away. Internal wave energy in regions with little local generation should

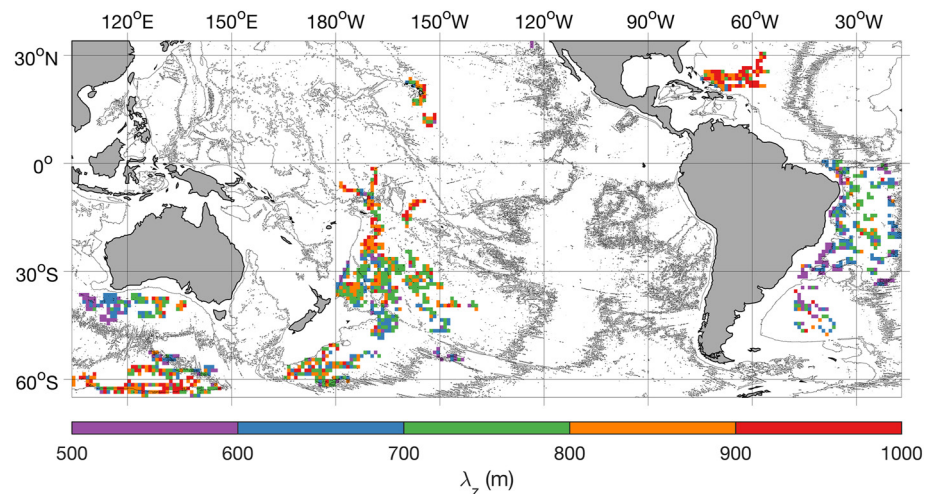


Figure 4. Dominant vertical wavelengths, λ_z , of w' from 1,000 m to the bottom pressure of deep SOLO profiles averaged in 1° latitude \times 1° longitude bins.

be relatively low, even for the longer vertical wavelength packets that survive traveling from remote generation regions. The few bins with higher $\sqrt{\langle w'^2 \rangle}$ s and smaller λ_z s near the continental slope may result from local interactions between currents and the bathymetry there.

In the Brazil Basin of the western South Atlantic $\sqrt{\langle w'^2 \rangle}$ s are largest and λ_z s shortest over the rough bathymetry of the Mid-Atlantic Ridge (Figures 2a, 3, and 4), where internal waves are generated. In contrast, over the smoother abyssal plain in the basin interior, $\sqrt{\langle w'^2 \rangle}$ s are smaller and λ_z s are longer, suggesting that there are few locally generated internal waves, leaving only attenuated low-mode internal waves that may have been generated elsewhere. This pattern is consistent with previous observations of a ridge-to-basin gradient in mixing in the Brazil Basin (Polzin et al., 1997) and with strain and shear variances from WOCE section data in many basins (Kunze et al., 2006). Further west, approaching the continental slope, λ_z s become shorter while $\sqrt{\langle w'^2 \rangle}$ s remain small, suggesting that while there is little local generation, the continental slope may be reflecting or scattering internal waves, a pattern consistent with modeling studies of the internal wave lifecycle (e.g., de Lavergne et al., 2019). The shorter λ_z s near the slope could also arise partly owing to the shorter profiles taken there not resolving energy at longer wavelengths. In the Argentine Basin λ_z s are often short and $\sqrt{\langle w'^2 \rangle}$ s are moderate to strong, consistent with the deep-reaching eddies and currents in the region (e.g., Fu, 2007) interacting with the internal wave field in a variety of ways including acting as a conduit for surface-generated internal waves (Danioux et al., 2008; Kunze, 1985; Young & BenJelloul, 1997), or causing a reduction in the internal wave length scales via interactions with the currents vorticity or horizontal strain (Fer et al., 2018; Kunze, 1995).

The $\sqrt{\langle w'^2 \rangle}$ s (Figure 3) in the South Australian and Australian-Antarctic basins of the far eastern Indian Ocean are generally lower than average, especially in smooth regions, with some high values and shorter λ_z s (Figure 4) closer to bathymetric features. Just to the east, profiles south of the Campbell Plateau in the South Pacific have relatively high $\sqrt{\langle w'^2 \rangle}$ s and a variety of λ_z s. The deep-reaching Antarctic Circumpolar Current flows eastward through this region after transiting some very rough bathymetry to the west. Deep-reaching meanders and eddies of that current generating lee waves when flowing over that bathymetry (Cusack et al., 2017; Waterman et al., 2013) may be responsible for some of those high $\sqrt{\langle w'^2 \rangle}$ s.

In the Southwest Pacific Basin, $\sqrt{\langle w'^2 \rangle}$ s (Figures 2d and 3) are close to average in many locations, with higher values adjacent to the steep bathymetry of the Tonga-Kermadec Ridge and Trench system and around regions with rough bathymetry, including the chain of seamounts comprising the Louisville Ridge. The lower $\sqrt{\langle w'^2 \rangle}$ s to the north of that ridge in the center of the basin are in a region of smoother bathymetry, and again the λ_z s (Figure 4) tend to be longer there, consistent with propagation from remote forcing areas of most internal waves and weaker mixing found in that region.

Moving northward in the Pacific, $\sqrt{\langle w'^2 \rangle}$ s (Figures 2c and 3) are substantially higher than average within and immediately north of the Samoan Passage and in the Penrhyn Basin east of the Manihiki Plateau. The Samoan Passage is a constriction for northward flow of bottom water into the rest of the Pacific, with hydraulic jumps and strong mixing observed locally (Carter et al., 2019). The high values continuing farther to the north of the Passage and east of the Manihiki Plateau are perhaps partly owing to relatively rough bathymetry in those regions. Values are also high for the few floats in the North Pacific, all of which are close to rough bathymetry. Moving from South to North these floats are found in the Clarion-Clipperton Fracture Zone, around the Hawaiian Islands, and off the continental slope just west of San Diego.

4. Summary and Discussion

Internal wave signatures are apparent in variations of descent rate data (w') from Deep SOLO floats. Bin averaged $\sqrt{\langle w'^2 \rangle}$ s (Figure 3) and λ_z s (Figure 4) exhibit geographical variability tied to proximity to rough bathymetry and deep currents, with variations among and even within some deep basins. For example, within the Brazil Basin, $\sqrt{\langle w'^2 \rangle}$ s in the western part of the basin, where bathymetric roughness is very low on the abyssal plain, are on average about 3 times lower than those in the eastern part of the basin, where bathymetry is very rough on the western flank of the Mid-Atlantic Ridge. This result is consistent with earlier findings of increased microscale energy and mixing over mid-ocean ridges (Polzin et al., 1997). Another interesting contrast in $\sqrt{\langle w'^2 \rangle}$ s is the relatively high values found within the Samoan Passage compared to the lower values immediately to the south of that passage. This elevated activity could be partly owing to the influence of lee waves and hydraulic jumps as bottom water flows northward through the passage (Carter et al., 2019). The elevated $\sqrt{\langle w'^2 \rangle}$ s further north of

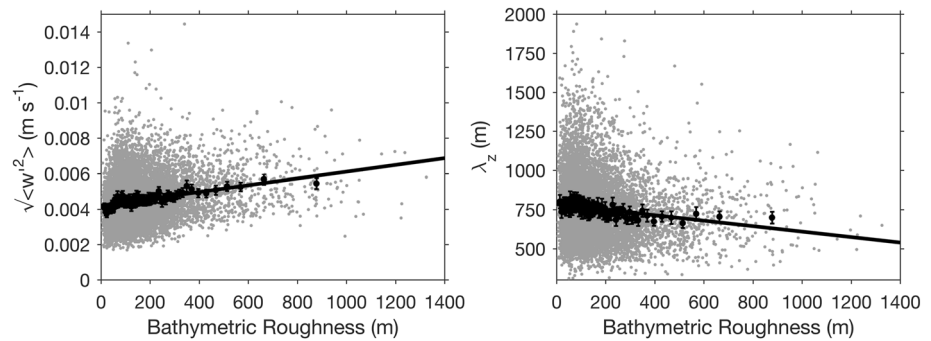


Figure 5. Scatter plots of (a) $\sqrt{\langle w'^2 \rangle}$ and (b) λ_z versus bathymetric roughness (gray dots) with linear fits (solid lines) and mean values of 94 profiles each binned according to bathymetric roughness with 2.5%–97.5% confidence limits (black dots with error bars).

the passage could also be partly owing to the interactions of tidal flows, which can propagate over long distances, especially those at low vertical modes (Zhao et al., 2016), with local rough bathymetry.

The $\sqrt{\langle w'^2 \rangle}$ s from individual profiles are correlated at 0.21 with bathymetric roughness (Figure 5a, gray dots). So, as expected, deep internal wave activity is higher in the vicinity of rough bathymetry. Furthermore, λ_z s from individual profiles are also correlated, at -0.14 , with local bathymetric roughness (Figure 5b, gray dots). This negative correlation is also expected as locally generated internal waves should have shorter vertical wavelengths than those propagating from more distant generation regions, because the shorter vertical wavelength packets are more subject to breaking and subsequent dissipation. The correlations are not high, probably because internal wave distributions are patchy, bathymetric roughness is poorly resolved in some regions, and deep currents and tides also contribute to local internal wave generation. However, bin averaging $\sqrt{\langle w'^2 \rangle}$ and λ_z values as a function of bathymetric roughness (Figure 5, black dots with error bars) greatly reduces uncertainties. The bin averaged values are in good agreement with linear fits (Figure 5, black lines) to the individual profile data.

Since float profiling rates typically take tens of seconds to adjust to changes in forcing including ambient vertical velocity, float buoyancy, and ambient density (e.g., Cusack et al., 2017), the perturbations in their descent rates will be slightly attenuated and lagged relative to the actual internal wave vertical velocities. However, even for shorter λ_z s (e.g., 493 m) and the fastest background float descent rates (e.g., 0.17 m s^{-1}), profiling for half a vertical wavelength would take around 24 min, far longer than float adjustment times. Hence, these measurement errors should have a very small impact on the results of this study.

For internal waves generated at the sea-floor, which would have group velocity (and energy) propagation upward, hence phase velocity (crest and troughs) propagation downward, sampling on descent would bias λ_z estimates toward long values by a Doppler effect. For such internal waves at the inertial period, the λ_z s estimated here at the latitudes reported would be biased long by $8 (\pm 4)\%$ for an average float descent rate of 0.12 m s^{-1} . If instead the energy propagation were always downward, the λ_z estimates would be biased short by $7 (\pm 3)\%$ at inertial periods. For internal waves with M2 tidal periods, these errors would be $17 (\pm 5)\%$ long and $13 (\pm 3)\%$ short. However, if energy propagation were evenly split between upward and downward packets, these errors would be random, and unbiased. At any rate, wave amplitudes are unaffected by this issue.

It would also be interesting to examine internal wave signatures in deep density vertical strain using the float CTD data (temperature, salinity, and pressure profiles), similarly to what has been done with core Argo data (Whalen et al., 2012). However, many of these Deep SOLO float CTDs were set to sample at 50 m intervals over some of the deeper portions of the water column to conserve float battery energy. Sampling at more frequent intervals (25 m would be sufficient) would be required to properly estimate the deep strain. Nonetheless, the data we have so far of deep w' variances provide a tantalizing glimpse of what might be learned of internal wave energy distributions in the deep ocean from a global Deep Argo array. Already, with only a few Deep Argo regional pilot arrays established, there are roughly three times the number of Deep Argo profiles than were used from all of WOCE in one study of deep mixing (Kunze et al., 2006). Setting all Deep Argo floats to collect CTD data at vertical separations of 25 m or less would benefit future studies on this topic.

Data Availability Statement

The Argo data used here, located in the trajectory (.traj) files, were collected and made freely available at <https://doi.org/10.17882/42182> by the International Argo Program and the national programs that contribute to it (Argo, 2021). The GEBCO bathymetry data (GEBCO Compilation Group, 2021) used are available at <https://doi.org/10.5285/c6612cbe-50b3-0cff-e053-6c86abc09f8f>.

Acknowledgments

Two anonymous reviewers made helpful suggestions. G. C. Johnson was supported by the NOAA Global Ocean Monitoring and Observation Program, NOAA Research, and the Paul G. Allen Family Foundation. C. B. Whalen by NSF Award OCE-1923558, and N. Zilberman and S. G. Purkey by SIO CIMEAS Argo and CORC (NOAA grant NA20OAR4320278) and NOPP (NOAA grant NA18OAR0110434). PMEL Contribution Number 5335.

References

- Alford, M. H., MacKinnon, J. A., Simmons, H. L., & Nash, J. D. (2016). Near-inertial internal gravity waves in the ocean. *Annual Review of Marine Science*, 8(8), 95–123. <https://doi.org/10.1146/annurev-marine-010814-015746>
- Argo. (2021). Argo float data and metadata from Global Data Assembly Centre (Argo GDAC). *SEANOE*. <https://doi.org/10.17882/42182>
- Carter, G. S., Voet, G., Alford, M. H., Girtton, J. B., Mickett, J. B., & Klymak, J. M. (2019). A spatial geography of abyssal turbulent mixing in the Samoan passage. *Oceanography*, 32(4), 194–203. <https://doi.org/10.5670/oceanog.2019.425>
- Cleveland, W. S., & Devlin, S. J. (1988). Locally weighted regression—An approach to regression-analysis by local fitting. *Journal of the American Statistical Association*, 83(403), 596–610. <https://doi.org/10.1080/01621459.1988.10478639>
- Cusack, J. M., Garabato, A. C. N., Smeed, D. A., & Girtton, J. B. (2017). Observation of a large lee wave in the drake passage. *Journal of Physical Oceanography*, 47(4), 79–810. <https://doi.org/10.1175/JPO-D-16-0153.1>
- Danioux, E., Klein, P., & Riviere, P. (2008). Propagation of wind energy into the deep ocean through a fully turbulent mesoscale eddy field. *Journal of Physical Oceanography*, 38(10), 2224–2241. <https://doi.org/10.1175/2008JPO3821.1>
- de Lavergne, C., Falahat, S., Madec, G., Roquet, F., Nycander, J., & Vic, C. (2019). Toward global maps of internal tide energy sinks. *Ocean Modelling*, 137, 52–75. <https://doi.org/10.1016/j.ocemod.2019.03.010>
- de Lavergne, C., Madec, G., Le Sommer, J., Nurser, A. J. G., & Naveira Garabato, A. C. (2016). On the consumption of Antarctic bottom water in the abyssal ocean. *Journal of Physical Oceanography*, 46(2), 635–661. <https://doi.org/10.1175/JPO-D-14-0201.1>
- Fer, I., Bosse, A., Ferron, B., & Bouruet-Aubertot, P. (2018). The dissipation of kinetic energy in the Lofoten Basin eddy. *Journal of Physical Oceanography*, 48(6), 1299–1316. <https://doi.org/10.1175/JPO-D-17-0244.1>
- Foppert, A., Rintoul, S. R., Purkey, S. G., Zilberman, N., Kobayashi, T., Sallée, J.-B., et al. (2021). Deep Argo reveals bottom water properties and pathways in the Australian-Antarctic Basin. *Journal of Geophysical Research: Oceans*, 126, e2021JC017935. <https://doi.org/10.1029/2021jc017935>
- Fu, L. (2007). Interaction of mesoscale variability with large-scale waves in the Argentine Basin. *Journal of Physical Oceanography*, 37(3), 787–793. <https://doi.org/10.1175/JPO2991.1>
- Garrett, C., & Munk, W. (1979). Internal waves in the ocean. *Annual Review of Fluid Mechanics*, 11, 339–369. <https://doi.org/10.1146/annurev.fl.11.010179.002011>
- GEBCO Compilation Group. (2021). *GEBCO 2021 grid*. <https://doi.org/10.5285/c6612cbe-50b3-0cff-e053-6c86abc09f8f>
- Gille, S. T., Yale, M. M., & Sandwell, D. T. (2000). Global correlation of mesoscale ocean variability with seafloor roughness from satellite altimetry. *Geophysical Research Letters*, 27(9), 1251–1254. <https://doi.org/10.1029/1999GL007003>
- Johnson, G. C., Cadot, C., Lyman, J. M., McTaggart, K. E., & Steffen, E. L. (2020). Antarctic bottom water warming in the Brazil Basin: 1990s through 2020, from WOCE to Deep Argo. *Geophysical Research Letters*, 47(18), e2020GL089191. <https://doi.org/10.1029/2020GL089191>
- Johnson, G. C., Lyman, J. M., & Purkey, S. G. (2015). Informing Deep Argo array design using Argo and full-depth hydrographic section data. *Journal of Atmospheric and Oceanic Technology*, 32(11), 2187–2198. <https://doi.org/10.1175/JTECH-D-15-0139.1>
- Johnson, G. C., Purkey, S. G., Zilberman, N. V., & Roemmich, D. (2019). Deep Argo quantifies bottom water warming rates in the Southwest Pacific Basin. *Geophysical Research Letters*, 46(5), 2662–2669. <https://doi.org/10.1029/2018GL081685>
- Kunze, E. (1985). Near-inertial wave-propagation in geostrophic shear. *Journal of Physical Oceanography*, 15(5), 544–565. [https://doi.org/10.1175/1520-0485\(1985\)015<0544:niwpg>2.0.co;2](https://doi.org/10.1175/1520-0485(1985)015<0544:niwpg>2.0.co;2)
- Kunze, E. (1995). The energy-balance in a warm-core ring's near-inertial critical layer. *Journal of Physical Oceanography*, 25(5), 942–957. [https://doi.org/10.1175/1520-0485\(1995\)025<0942:tebiaw>2.0.co;2](https://doi.org/10.1175/1520-0485(1995)025<0942:tebiaw>2.0.co;2)
- Kunze, E. (2017). Internal-wave-driven mixing: Global geography and budgets. *Journal of Physical Oceanography*, 47(6), 1325–1345. <https://doi.org/10.1175/jpo-d-16-0141.1>
- Kunze, E., Firing, E., Hummon, J. M., Chereskin, T. K., & Thurnherr, A. M. (2006). Global abyssal mixing inferred from lowered ADCP shear and CTD strain profiles. *Journal of Physical Oceanography*, 36(8), 1553–1576. <https://doi.org/10.1175/JPO2926.1>
- Munk, W., & Wunsch, C. (1998). Abyssal recipes II: Energetics of tidal and wind mixing. *Deep-Sea Research I*, 45(12), 1977–2010. [https://doi.org/10.1016/S0967-0637\(98\)00070-3](https://doi.org/10.1016/S0967-0637(98)00070-3)
- Nikurashin, M., & Ferrari, R. (2013). Overturning circulation driven by breaking internal waves in the deep ocean. *Geophysical Research Letters*, 40(12), 3133–3137. <https://doi.org/10.1002/grl.50542>
- Polzin, K. L., Toole, J. M., Ledwell, J. R., & Schmitt, R. W. (1997). Spatial variability of turbulent mixing in the abyssal ocean. *Science*, 276(5309), 93–96. <https://doi.org/10.1126/science.276.5309.93>
- Roemmich, D., Alford, M. H., Claustre, H., Johnson, K., King, B., Moum, J., et al. (2019). On the future of Argo: A global, full-depth, multi-disciplinary array. *Frontiers in Marine Science*, 6(439). <https://doi.org/10.3389/fmars.2019.00439>
- Roemmich, D., Sherman, J. T., Davis, R. E., Grindley, K., McClune, M., Parker, C. J., et al. (2019b). Deep SOLO: A full-depth profiling float for the Argo program. *Journal of Atmospheric and Oceanic Technology*, 36(10), 1967–1981. <https://doi.org/10.1175/JTECH-D-19-0066.1>
- Smith, W. H. F., & Sandwell, D. T. (1997). Global sea floor topography from satellite altimetry and ship depth soundings. *Science*, 277(5334), 1956–1962. <https://doi.org/10.1126/science.277.5334.1956>
- Thomas, G., Purkey, S. G., Roemmich, D., Foppert, A., & Rintoul, S. R. (2020). Spatial variability of Antarctic bottom water in the Australian Antarctic Basin from 2018–2020 captured by Deep Argo. *Geophysical Research Letters*, 47(23), e2020GL089467. <https://doi.org/10.1029/2020GL089467>
- Waterhouse, A. F., MacKinnon, J. A., Nash, J. D., Alford, M. H., Kunze, E., Simmons, H. L., et al. (2014). Global patterns of diapycnal mixing from measurements of the turbulent dissipation rate. *Journal of Physical Oceanography*, 44(7), 1854–1872. <https://doi.org/10.1175/JPO-D-13-0104.1>
- Waterman, S., Garabato, A. C. N., & Polzin, K. L. (2013). Internal waves and turbulence in the Antarctic circumpolar current. *Journal of Physical Oceanography*, 43(2), 259–282. <https://doi.org/10.1175/JPO-D-11-0194.1>

- Whalen, C. B., Talley, L. D., & MacKinnon, J. A. (2012). Spatial and temporal variability of global ocean mixing inferred from Argo profiles. *Geophysical Research Letters*, *39*, L18612. <https://doi.org/10.1029/2012GL053196>
- Young, W. R., & Jelloul, M. B. (1997). Propagation of near-inertial oscillations through a geostrophic flow. *Journal of Marine Research*, *55*(4), 735–766. <https://doi.org/10.1357/0022240973224283>
- Zhao, Z. X., Alford, M. H., Girton, J. B., Rainville, L., & Simmons, H. L. (2016). Global observations of open-ocean mode-1 M-2 internal tides. *Journal of Physical Oceanography*, *46*(6), 1657–1684. <https://doi.org/10.1175/JPO-D-15-0105.1>
- Zilberman, N. V., Roemmich, D. H., & Gilson, J. (2020). Deep-ocean circulation in the southwest Pacific Ocean interior: Estimates of the mean flow and variability using Deep Argo data. *Geophysical Research Letters*, *47*(13), e2020GL088342. <https://doi.org/10.1029/2020GL088342>